KEK Preprint 97-89
June 1997
A

Dynamic Aperture for High-Brilliance Optics of the Photon Factory Storage Ring

E.-S. KIM, Y. KOBAYASHI and M. KATOH

Submitted to Japanese Journal of Applied Physics

** From April 1, 1997, **High Energy Accelerator Research Organization (KEK)** was newly established. The new organization is restructured of three reseach institutes, National Laboratory for High Energy Physics (KEK), Institues of Nuclear Study (INS), Univ. of Tokyo and Meson Science Laboratory, Faculty of Science, Univ. of Tokyo.*

High Energy Accelerator Research Organization (KEK), 1997

KEK Reports are available from:

Information Resources Division
High Energy Accelerator Research Organization (KEK)
1-1 Oho, Tsukuba-shi
Ibaraki-ken, 305
JAPAN

Phone: 0298-64-5137
Fax: 0298-64-4604
Cable: KEK OHO
E-mail: Library@kekvax.kek.jp (Internet Address)
Internet: http://www.kek.jp

Dynamic Aperture for High-Brilliance Optics of the Photon Factory Storage Ring

Eun-San Kim, Yukinori Kobayashi and Masahiro Katoh
High Energy Accelerator Research Organization (KEK)
1-1 Oho, Tsukuba, Ibaraki, 305, Japan

Abstract

The dynamic apertures in several lattices for the low emittance of the PF ring have been investigated by a simulation method using the code SAD. The dynamic apertures in each lattice without and with machine errors were obtained by a tune survey in the simulation. It was also shown how large are the dynamic apertures compensated after corrections of a closed orbit distortions. The operating tunes in low-emittance lattices can be obtained based on the view point of dynamic apertures obtained from a tune survey. It is shown that a low-emittance 90° cell lattice provides sufficient dynamic aperture after a correction of the closed orbit distortion in the PF ring.

1 Introduction

The PF ring is a light source using the 2.5 GeV electron storage ring which has been operated since 1982. A high-brilliance project at the PF ring is in progress. By the project, the light source is designed to produce smaller beam emittances that can provide more brilliant synchrotron radiation. The present beam emittance of 130nm-rad in the PF ring was obtained by changing the strenghts of the quadrupoles in 1986. However, this emittance is still larger by ten times than third generation synchrotron light sources; also the brilliance of the synchrotron radiation beam from the insertion devices is smaller by one or two orders of magnitude[1,2]. A greater emittance reduction in the PF-ring was required to compete with the third generation synchrotron light sources. It was shown that the beam emittance in the present PF-ring could be reduced to 27 nm-rad by doubling the number of quadrupole and sextupole magnets in the FODO cells, which consist of the normal cell sections. This can lead to a higher brilliance of the synchrotron radiation. However, we are faced with the fact that the strong quadrupole and sextupole magnets which are necessary to provide small emittance can affect the beam dynamics in this light source.

The focal properties of a FODO lattice depend on the quadrupole's strengths. Thus, the linear chromaticity due to the quadrupoles can become negatively larger for a machine of low-emittance which requires strong strenghts of the quadrupoles. This fact is shown in Table-1. Here, the lattices for three cases of phase advance (90°, 105° and 135°) for low-emittance are considered, and medium means the present optics in the PF ring. Two sextupole families are then used to compensate for these chromaticities in the horizontal and vertical planes. Compensation of the chromaticity can be effectively performed when the sextupoles are set to the positions where the dispersion function and betatron function are large. Thus, we set the focusing sextupoles(SF) and defocusing sextupoles(SD) near to the focusing quadrupoles and defocusing quadrupoles, respectively. However, sextupoles of strong strengths are required, since the dispersion function and betatron function are small in a low-emittance ring. The strengths of the sextupoles for two families compensation in the PF ring are also given in Table-1. Then, it is necessary to notice the effects of a nonlinear magnetic field due to the strong sextupoles to compensate for the chromaticity[3]. These effects can affect the motions of a particle with large amplitude and large momentum deviation. Thus, unstable motion can suddenly occur in a particle with amplitudes higher than any amplitude. This undesirable behavior leads to beam loss and affects the beam lifetime. It may greatly affect the machine operation.

Since low-emittance lattices in the PF ring require ten-times stronger sextupoles than the present one, we can see that the dynamic aperture becomes smaller. Accordingly, it is desirable to investigate the dynamic apertures in low-emittance lattices which are affected by strong sextupoles. It is necessary to estimate how a sufficient dynamic aperture for beam injection and storage into the ring can be obtained in low-emittance lattices. This was a motivation of this study. From predicting of the computer simulation using a model of an ideal machine without any errors, it was shown that we could obtain a low-emittance lattice in which the dynamic aperture is

larger than the physical aperture[4]. Since a real machine has various imperfections, however, it is required to estimate the dynamic aperture in a machine which includes various errors. Since closed orbit distortions(COD) are corrected by steering dipole and bending magnets in the PF ring, it is also necessary to investigate how large the dynamic apertures in low-emittance lattices are compensated by corrections of the COD.

Accordingly, we investigated in detail the dynamic aperture for three lattices of low-emittance and a medium emittance by a simulation method. The simulation was performed using the computer code SAD[5], which has been developed at KEK. The dynamic aperture in this simulation is defined as the maximum initial amplitude to give a circulation of 1000 turns. The simulation first shows the dynamic aperture for an ideal lattice without any errors. It then shows the dynamic aperture when some typical machine errors are included to the lattices. Errors due to the magnetic field, alignment, rotation, length, kick of steering magnet and beam position monitor are considered to be machine errors in the simulation. The dependence of the dynamic aperture on an individual machine error is also shown. We then also investigate how large dynamic apertures due to corrections of the COD are recovered in each lattice. The dynamic apertures are obtained by scanning the betatron tunes within a specified tune space. Accordingly, we can choose the operating tune in each lattice from the dynamic apertures obtained by a tune survey. Based on this estimation, we can find low-emittance optics whose dynamic aperture becomes large enough for injection and storage of the beam into the ring. As a result, the emittance which can be achieved in the PF ring is determined in terms of the dynamic aperture. In the next section, we give an overview of the machines for low and medium emittances of the PF ring. Sec.3 gives a general illustration of the dynamic aperture. The dynamic apertures which result from a tune survey for several optics are shown in Sec.4. The last section is devoted to a discussion and the results.

2 Machine Overview

Let us overview the machine for both new and present lattices[1,2]. The basic lattice structure of the PF ring is FODO. The normal cells, which occupy one third of the ring and determine the beam emittance, will be changed for higher brilliant synchrotron radiation. The bending magnets will not be changed. This would minimize the influence on the existing beam lines of synchrotron radiation. The quadrupoles and sextupoles in the normal cells are doubled in number and reinforced in strength by two and ten times, respectively[4]. Thus, all of the quadrupoles and sextupoles in the normal cells will be replaced by new ones having higher field gradients. The maximum field gradients are compatible with 3 GeV operation with the lowest emittance optics. The sextupoles have auxiliary windings for vertical steering. They can be used to produce skew quadrupole fields to control the coupling constant.

The optics of the whole ring was designed for the three cases of the horizontal phase advance: 90^o, 105^o and 135^o. In the case of 135^o, we obtain the lowest emittance of 27 nm-rad. A higher brilliance of synchrotron radiation at the present beam lines will be given by a factor of 5 to 10 from these three optics.

Typical parameters in low and medium emittances are given in Table-1. Here, 90^o, 105^o and 135^o cell optics are the new high brilliance optics. The medium cell optics is the similar one before the emittance upgrade. Here, H and V mean the horizontal and vertical directions, respectively. The strengths($1/m^2$) of the focusing and defocusing sextupole magnets to correct the chromaticities are also given.

3 Dynamic Aperture

The dynamic aperture gives a description of the nonlinear effects arising from sextupoles to correct for the chromaticity and field imperfections of the magnets[6]. In this stage of the design, it is necessary to estimate how large is the dynamic aperture of such a machine and how large is the dynamic aperture recovered by a correction of the COD. It is analytically difficult to obtain the dynamic aperture in the presence of nonlinear fields and thus in general it is obtained by a simulation method. The dynamic aperture is determined in a simulation as follows: first, set the initial amplitude of the betatron oscillation and track its amplitude through the ring's components. If the initial amplitude performs stable betatron oscillation within a region until given turns, we assume that a particle with its amplitude can infinitely perform stable betatron oscillation. Whether the initial amplitude can perform stable betatron oscillation until the given turns or not, we call this boundary value of its initial amplitude to the dynamic aperture. In electron storage rings, because an initial large amplitude dampens its amplitude by synchrotron radiation, we assume that 1000 turns is sufficient as a condition of stable betatron oscillation. Accordingly, we will investigate the dynamic aperture by tracking 1000 turns in our simulation.

Next, we discuss how we evaluate the dynamic apertures which are obtained by a simulation method. In the high brilliance lattices of the PF ring, the

horizontal and vertical directions are most limited by the duct of the superconducting vertical wiggler-VW 14 and the duct of multipole wiggler-MWP 16 at the long straight line, respectively. Accordingly, the physical aperture is determined by these ducts of insertion devices. When we consider the physical aperture as sizes of these ducts, the physical aperture in the PF ring becomes 15 mm and 7.5 mm at the horizontal and vertical directions in the long straight line, respectively. From a comparison of this physical aperture and the dynamic aperture, which is obtained by a simulation method, we can determine whether the dynamic aperture provided by a lattice can lead to stable motion of the beam or not.

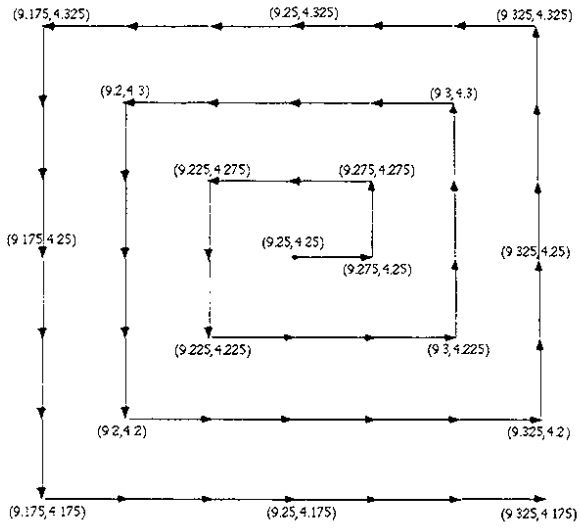

Figure 1: Tune variation in the tune survey to obtain the dynamic apertures in 90° cell optics. The tune scan starts from a tune (9.25, 4.25). The variation in the tune is performed by 0.025 per a step in the horizontal and vertical tunes, respectively.

4 Tune Survey

The dynamic aperture has a deep relation with the betatron tune. It is difficult to obtain analytically betatron tunes which enable us to provide a large dynamic aperture. To obtain a betatron tune which gives a large dynamic aperture, the only method is to check the dynamic aperture by changing the betatron tunes. Therefore, by changing the betatron tunes it is possible to obtain a reasonable operating point which gives a large dynamic aperture.

We perform tune survey for several optics. The following method is applied for this tune survey: 1)The fractional tune is changed from the starting point, which is given by (0.25,0.25). 2)The tune is fixed at quadrupoles of the normal cell to make the phase advance constant, and is changed at the quadrupoles of the straight line. In this way, matching of the optics is performed. 3)The variation in the tune is done by 0.025 in a step. The tune survey is performed over the range between 0.0 and 0.5 in the horizontal and vertical directions, respectively. Accordingly, the tune survey covers a rectangular region in tune space ($0 \leq \nu_x \leq 0.5$ and $0 \leq \nu_y \leq 0.5$). Within this region we scan 21 horizontal tune values by 21 vertical tune values. As an example, the tune survey in a 90° optics cell is performed as shown in Figure 1. 4) The dynamic aperture is obtained by averaging five points in the X-Y plane, as shown in Figure 2. The tracking turn is 1000 turns.

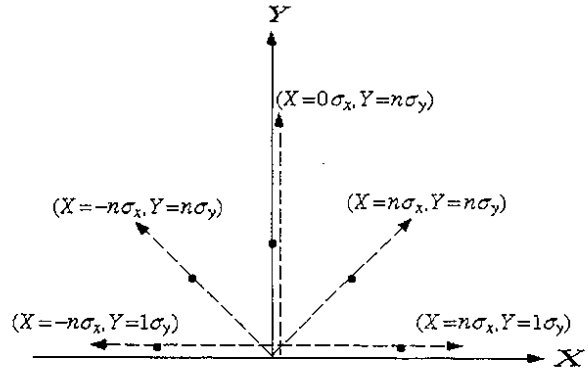

Figure 2: Survey of the dynamic aperture in the X-Y plane. The dynamic aperture is obtained by averaging these five points.

4.1 Low-Emittance 90° Cell Optics

Figure 3 shows the optics of a low-emittance 90° cell and its optical functions. Figure 4.(a) shows the dynamic aperture in the case that machine errors are not included. The magnitude of the dynamic aperture is expressed in unit of beam size, and is shown as the average value of five points in the X-Y plane, as shown in Figure 2. The particle momentum is kept at $\delta P/P$=0 during tracking. The tune plots showing the second-order, third-order and fourth-order resonances are presented by the heavy line, straight line and dashed lines, respectively, in Figure 4.(a). It is shown that the dynamic aperture becomes small near to the third-order resonance($3\nu_x$=28, $\nu_x+2\nu_y$=18). It is well known that these resonances are strongly generated when sextupoles are introduced into the ring. Here, we can also check this fact by tracking. Figure 4.(b) shows the dynamic aperture in the case

that the machine errors are included in Figure 4.(a). The magnitudes of the errors considered in the simulation are listed in Table-2. The errors are assumed to have a Gaussain distribution with the r.m.s values given in Table-2, and have been truncated by 3σ in their distributions. Figure 4.(b) shows smaller dynamic apertures than those of the case without machine errors. The third-order structure resonances are observed in the case without errors, while in the case with errors, a structural sum resonance is strongly excited. After corrections of the COD in Figure 4.(b) are performed, we can see that significant changes are observed in the performance of the dynamic aperture, as shown in Figure 4.(c).

On the other hand, when the machine errors are included into the lattice, we see that the tune is slightly changed. After a correction of the COD is performed, quadrupoles are adjusted to make a varied tune to the initial tune in the case of Fig.4.(c). Figure 4.(d) shows the dynamic apertures in the case that the tunes varied by machine errors are not set to the initial values after corrections of the COD. We see that Figures 4.(c) and (d) show almost the same result. This result is caused by the fact the tune variation due to machine errors is very small.

We can obtain a comparative large dynamic aperture around (ν_x=9.1, ν_y=4.1) in Fig.4.(a). However, we notice that there is a $\nu_x - \nu_y$=5 resonance near to this tune. By selecting ν_x=9.13 and ν_y=4.19, we investigated the dynamic aperture in the X-Y plane. Figure 5 shows the dynamic apertures at this tune at the center of a long straight section. Figure 5.(a) shows the dynamic apertures without machine errors. The dynamic apertures are shown in the cases of -1%, 0% and 1% momenta deviations. We can see that the dynamic apertures decrease for off-momentum particles. The dynamic aperture for a 0% momemtum deviation is larger than the physical aperture. The dynamic apertures in -1% and 1% momenta deviations show almost the same magnitudes as the physical aperture in the horizontal direction. Figure 5.(b) shows the dynamic apertures with machine errors. Figure 5.(c) the shows dynamic apertures after corrections of COD are applied in Figure 5.(b). It shows that the dynamic apertures are larger than the physical aperture in the horizontal and vertical directions. The COD in Figure 5.(c) is adjusted to an r.m.s. error of $0.37mm$ and $0.07mm$ in the horizontal and vertical directions, respectively. The dynamic apertures in Figure 5.(c) show the same tendency with Figure 5.(a).

We next show the dependence of the dynamic aperture on seeds of random numbers which are used for distributins of machine errors. Figure 6 shows the dynamic apertures when different seeds in random numbers are used in the case of Figure 5.(c). We find

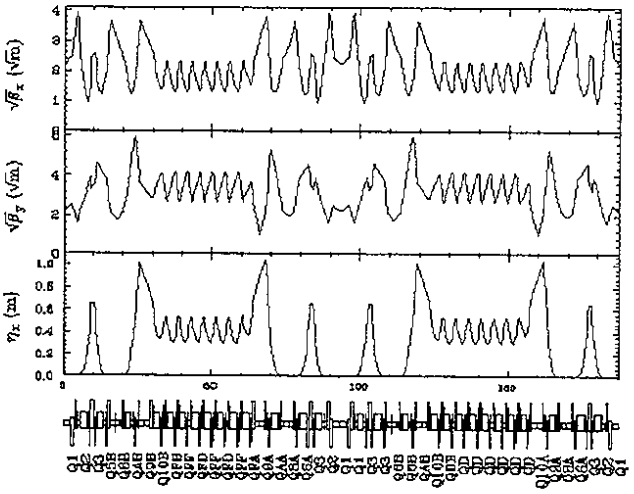

Figure 3: Low-emittance 90° cell and its optical functions.

that they have a similar global structure in different seeds.

It is important to show how large dynamic apertures in a ring with machine errors are recovered by a correction of the COD. Figures 7.(a) and (b) show the closed orbit distortions in the horizontal and vertical directions for the cases of 150 tunes in 90° optics, respectively. The points are closed orbit distortions when the machine errors are included to the ideal lattice. The circles are the closed orbit distortions after corrections of the COD in points are performed. We can see that the closed orbit distortions in the horizontal and vertical directions are adjusted to r.m.s. errors of 0.5mm and 0.2mm, respectively. It is shown that corrections of the COD are better performed in the vertical direction than in the horizontal direction.

From these results, we can expect that the PF ring has a sufficent dynamic aperture after a correction of the COD in the 90° cell optics, if the machine errors are kept within the level given in Table-2.

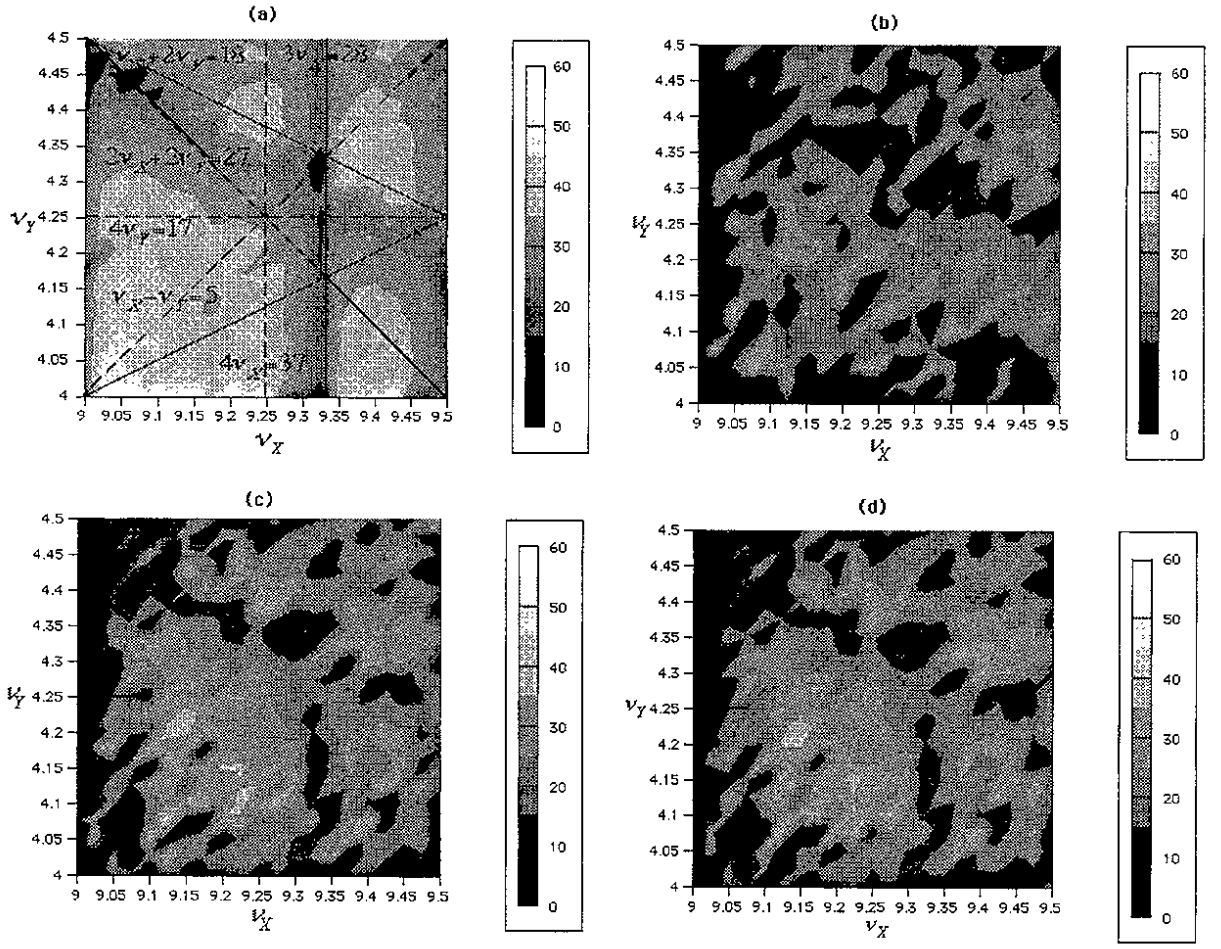

Figure 4: Dynamic apertures for a tune survey in 90° low-emittance cell optics. (a) Without machine errors, (b) With machine errors, (c) and (d) after corrections of COD in (b). (c) The tunes which are changed by machine errors are set to the initial values after corrections of COD. (d) The tunes are not set to the initial values after corrections of COD.

Table-1: Principal parameters for low-emittance optics and medium-emittance optics

Cell Optics	90^o	105^o	135^o	Medium
Natural emittance($nmrad$)	45.1	35.9	27.5	129.7
Betatron Tune(H/V)	9.15/4.25	9.66/4.25	10.83/4.23	8.36/3.21
Linear Chromaticity(H/V)	-11.85/-11.69	-12.54/-12.29	-16.04/-13.52	-13.64/-8.40
Strength of Sextupole(SF/SD)	6.39/-6.24	7.50/-7.39	9.69/-9.83	0.980/-1.58
RF Voltage (MV)	1.7	1.7	1.7	1.7
RF Bucket Height (%)	1.08	1.22	1.46	0.75

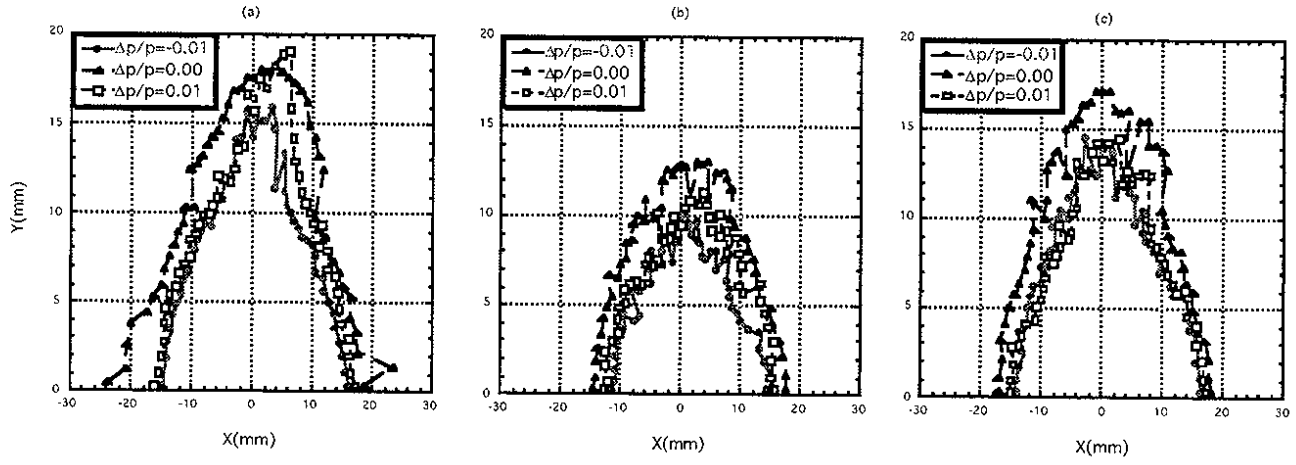

Figure 5: Dynamic apertures at the center of the long straight section. ν_x=9.13. ν_y=4.19. (a) Without machine errors, (b) With machine errors and (c) after corrections of COD in (b).

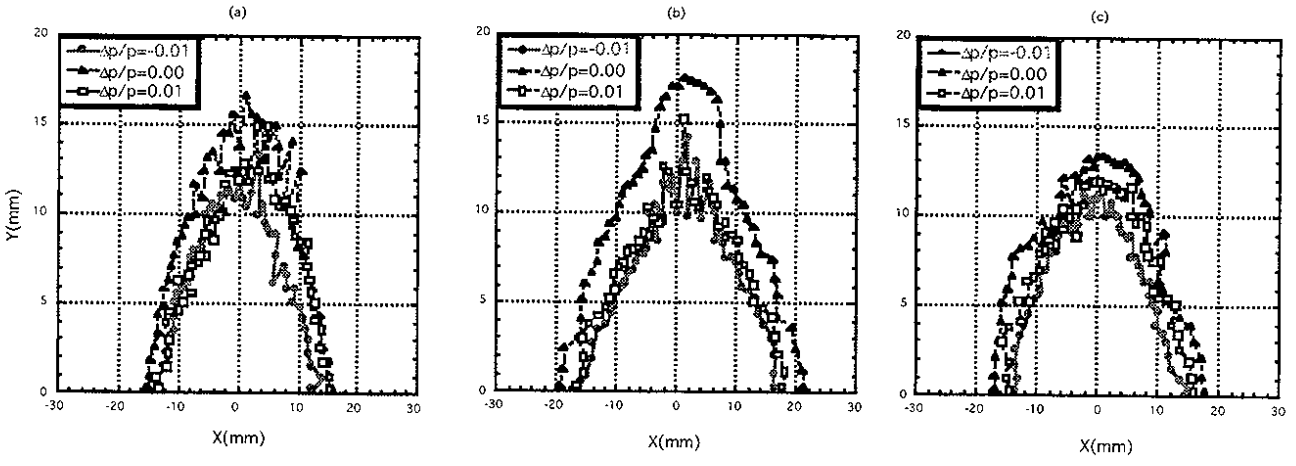

Figure 6: They show the dynamic apertures when other seeds of random numbers, in machine errors are used in the case of Figure 5.(c).

Table-2: Machine errors in a lattice

Magnet	Quadrupole	Bend	Sextuploe
Magnetic Field Error(RMS) (%)	0.1	0.1	0.2
Alignment Error(RMS) (Δ X/ΔY)(mm)	0.2/0.1		0.4/0.2
Rotation Error(RMS) (mrad)	0.2	0.2	0.2
Length Error(mm)	1	1	1
Steering Magnet(0.01%), BPM Error(offset:0.1mm, resolution:0.01mm)			

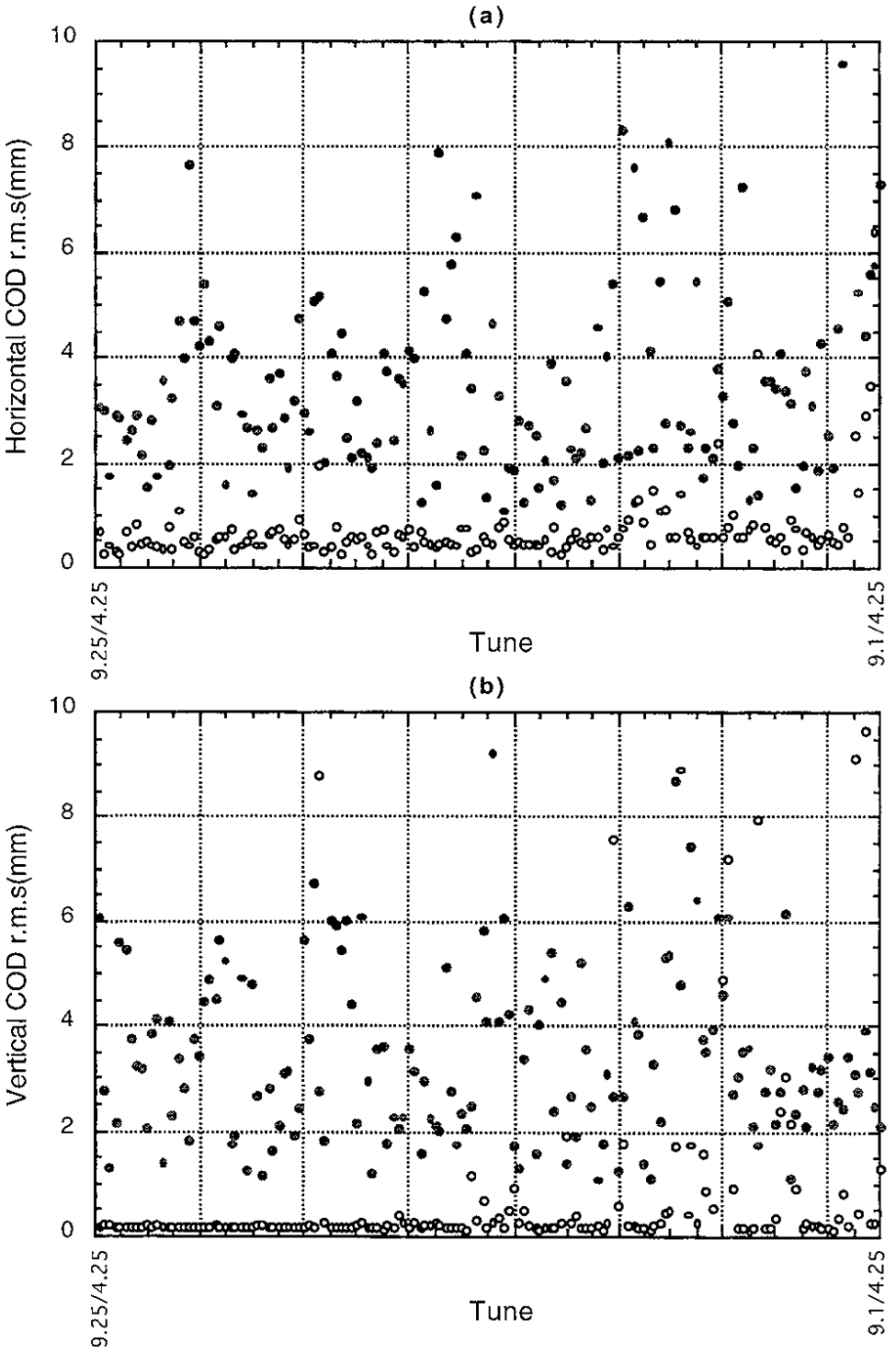

Figure 7: (a) and (b) show the horizontal and vertical COD for tunes in 90^o optics, respectively. Here, the points are the COD when the machine errors are included to the ideal lattice. The circles are the COD after corrections of the COD in points are performed. 150 tunes are given according to tune survey shown in Figure 1.

4.2 Low-Emittance 105° Cell Optics

Figure 8 shows the optics of a low emittance 105° cell and its optical functions. Figure 9.(a) shows the dynamic apertures obtained from tune survey when the machine errors are not included in the lattice. A tune plot showing the resonances lines is also presented by second order(heavy line), third order (straight line) and fourth order (dashed lines). A strong resonance is driven by the third order resonance($\nu_x+2\nu_y=18$). It is shown that the dynamic apertures become small near to this resonance. Figure 9.(b) shows the dynamic apertures in a tune survey when the machine errors are included in the lattice. Figure 9.(c) shows the dynamic aperture after corrections of the COD are performed in Figure 9.(b).

We can obtain a comparative large dynamic aperture at around (ν_x=9.61, ν_y=4.26). At this tune, we investigated the dynamic apertures in the X-Y plane. Then, Figure 10 shows the dynamic apertures at the center of the long straight section at this tune. Figure 10.(a) shows the dynamic apertures without machine errors. In the case that there is no deviation in the momentum, the dynamic aperture is greater than the physical aperture. The off-momenta, horizontal apertures have almost the same magnitude as the physical aperture. Figure 10.(b) shows the dynamic apertures with machine errors. Figure 10.(c) shows the dynamic apertures after corrections of the COD are applied in Figure 10.(b). Large changes are observed in the performance of the dynamic aperture. However, the horizontal apertures after corrections of the COD become even less than the physical aperture, even if there is no deviation in the momentum. The COD in Figure 10.(c) is adjusted to an r.m.s. error of $0.40mm$ and $0.08mm$ in the horizontal and vertical directions, respectively. Totally, 105° cell optics gives even smaller dynamic apertures than that of 90° cell optics.

Figures 11.(a) and (b) show the closed orbit distortions in the horizontal and vertical directions for the cases of 150 tunes in 105° optics, respectively. The points show the closed orbit distortions when the machine errors are included to ideal lattice. The circles show the closed orbit distortions after corrections of the COD in points are performed. We can see that the COD in Figure 11 is adjusted to an r.m.s. error of 0.5mm and 0.2mm in the horizontal and vertical directions, respectively.

4.3 Low-Emittance 135° Cell Optics

Figure 12 shows the optics of low-emittance 135° cell and its optical functions. Figure 13.(a) shows the dynamic apertures for a tune survey in the case that the machine errors are not included in the lattice. Figure 13.(b) shows the dynamic apertures with machine errors. Figure 13.(c) the shows the dynamic apertures after corrections of the COD in Figure 13.(b). In this optics the dynamic apertures are totally narrow. Even if we choose the tune ν_x=10.60 and ν_y=4.35, which gives a comparative large dynamic aperture, the dynamic apertures in this tune are small, as shown in Figure 14. Even if there is no variation in the momentum, the dynamic aperture in the horizontal direction after the COD correction is still smaller than the physical aperture. Accordingly, we can see that the beam lifetime is greatly limited by the dynamic aperture in the case of 135° cell optics.

In Figure 14.(b) the dynamic aperture shrinks to 0. Here, it is worth noting the dependence of the dynamic aperture on the machine errors. Figure 15 shows the characteristic aspects that an individual machine error affects the dynamic aperture. As an example, Figure 15.(a) shows the dynamic aperture when a steering error is excluded in Figure 14.(b). It is shown from Figure 15.(f) that an alignment error among the machine errors gives the greatest effect to the dynamic aperture. It is also shown that the length error and the BPM error almost have no an effect on the dynamic aperture. Based on this simulation, it is critical to keep the misalignment error small.

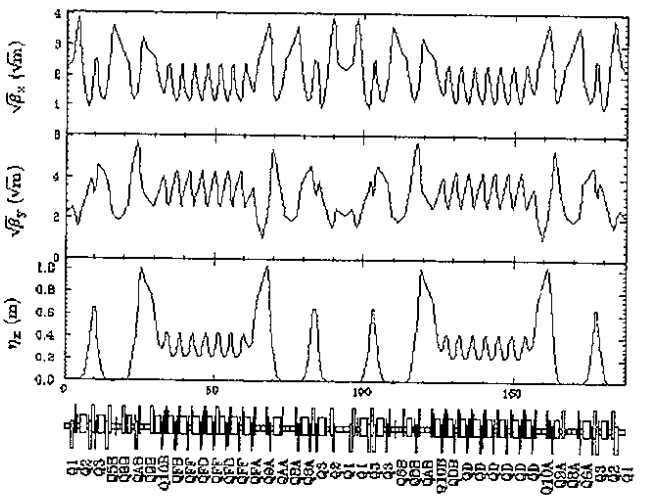

Figure 8: Low-emittance 105° cell and its optical functions

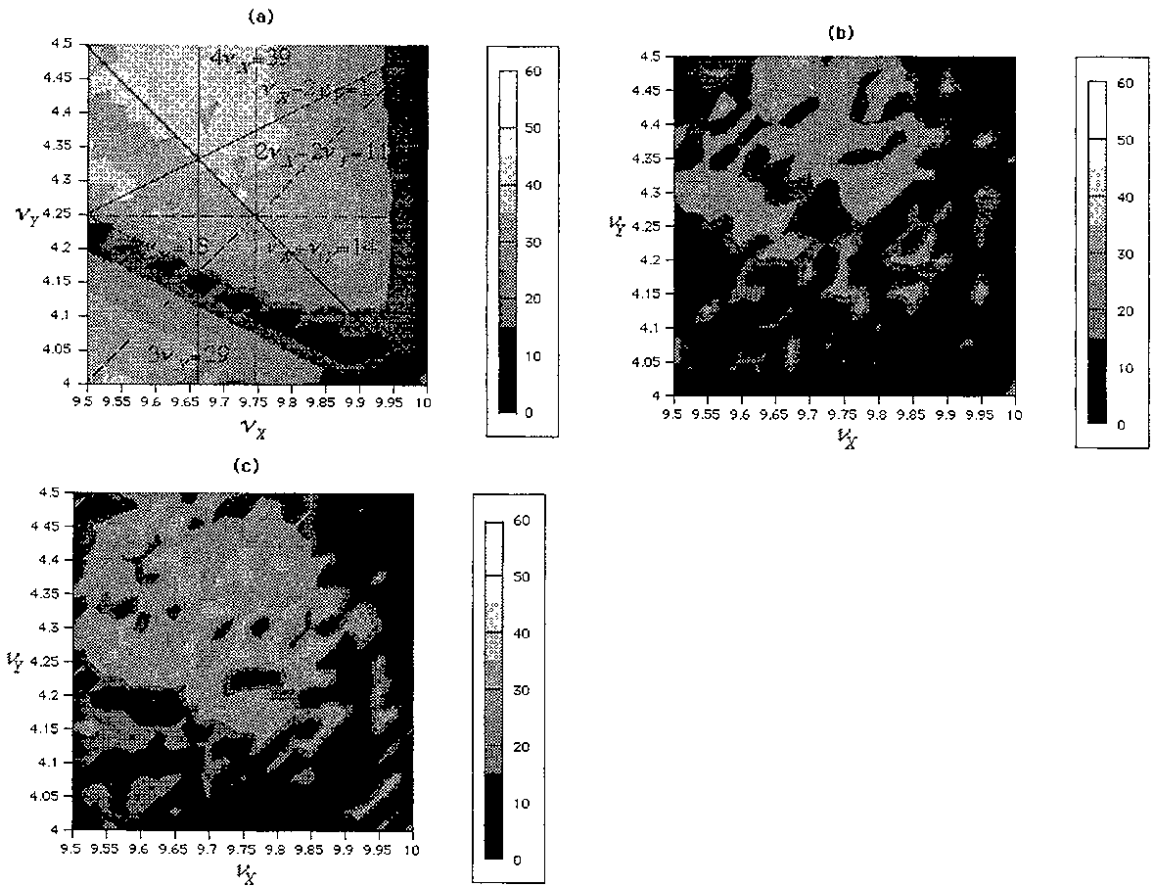

Figure 9: Dynamic apertures for a tune survey in 105° low-emittance cell optics. (a) Without machine errors, (b) with machine errors and (c) after corrections of the COD in (b).

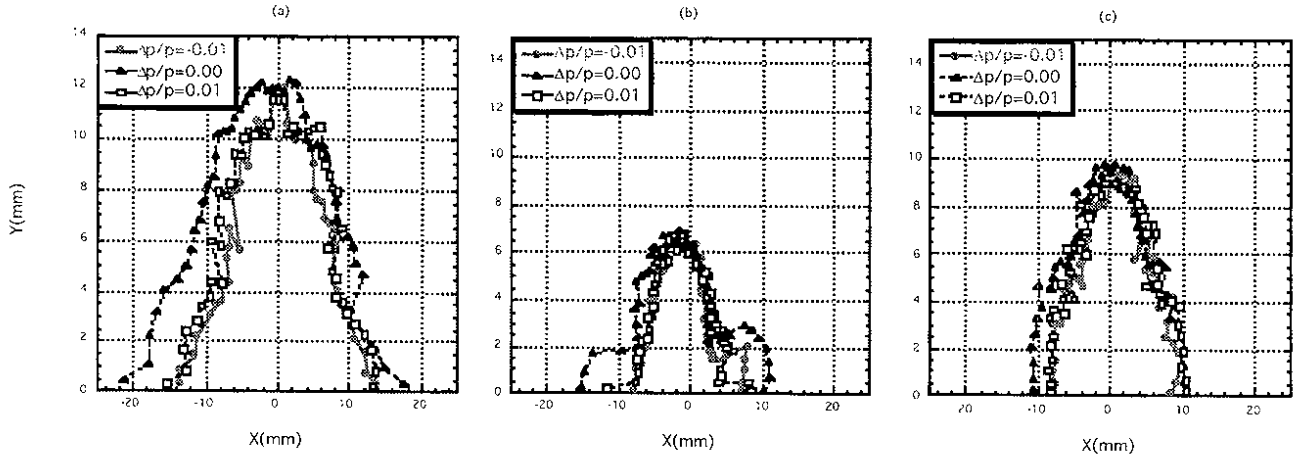

Figure 10: Dynamic apertures at the center of the long straight section in 105° low-emittance cell optics. (a) Without machine errors, (b) with machine errors and (c) after corrections of COD in machine errors. ν_x=9.61 and ν_y=4.26.

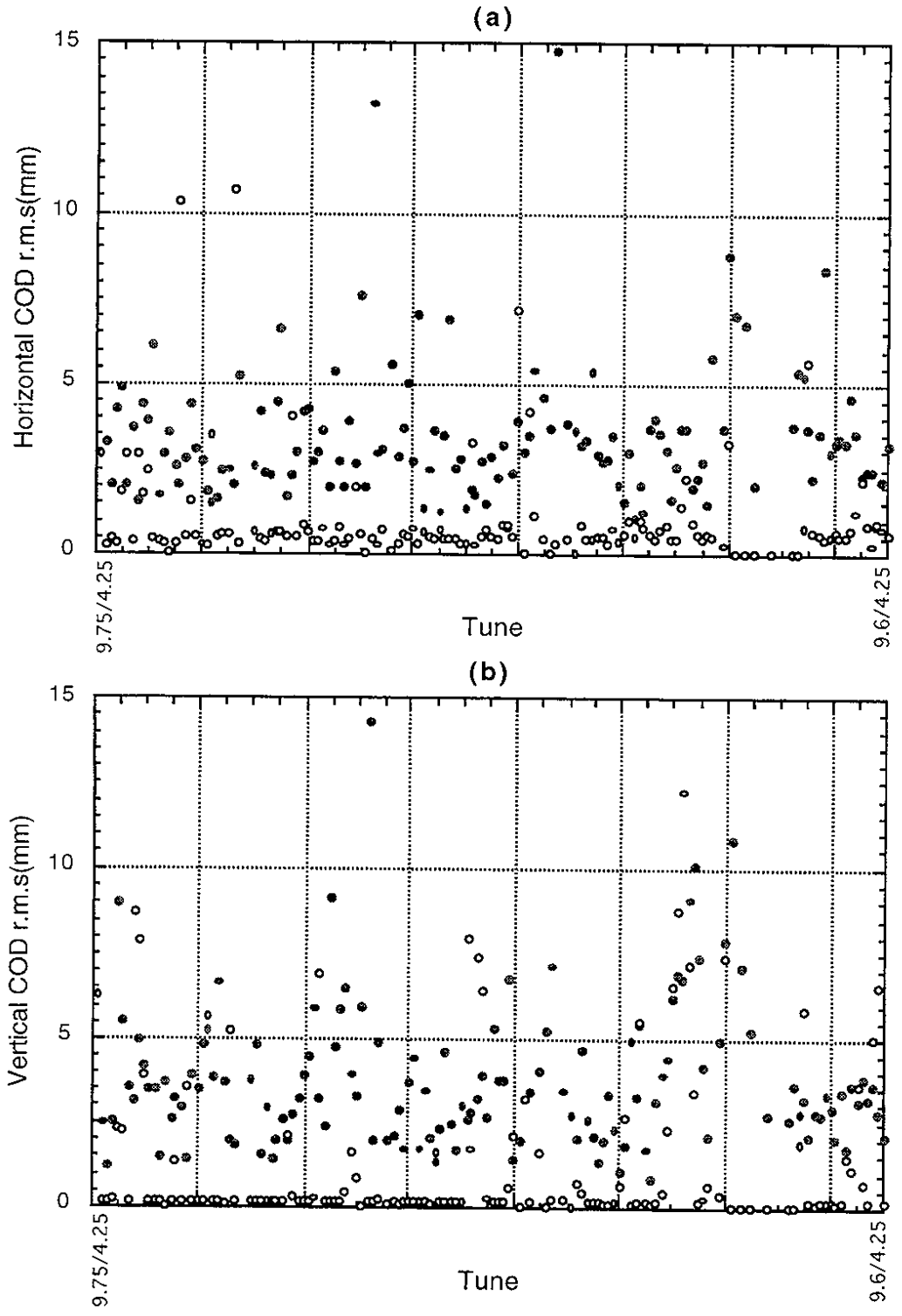

Figure 11: (a) and (b) show the horizontal and vertical COD for the cases of 150 tunes in 105° optics, respectively. Here, the points are the COD when the machine errors are included to the ideal lattice. The circles are the COD after corrections of the COD in points are performed.

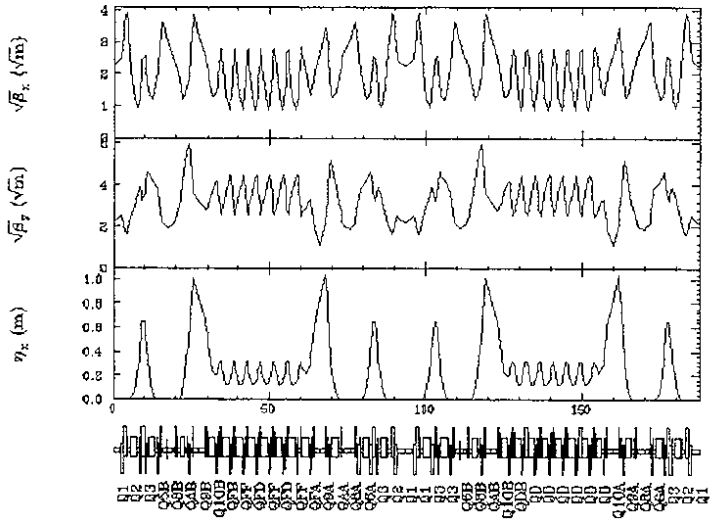

Figure 12: Low-emittance 135° cell and its optical functions

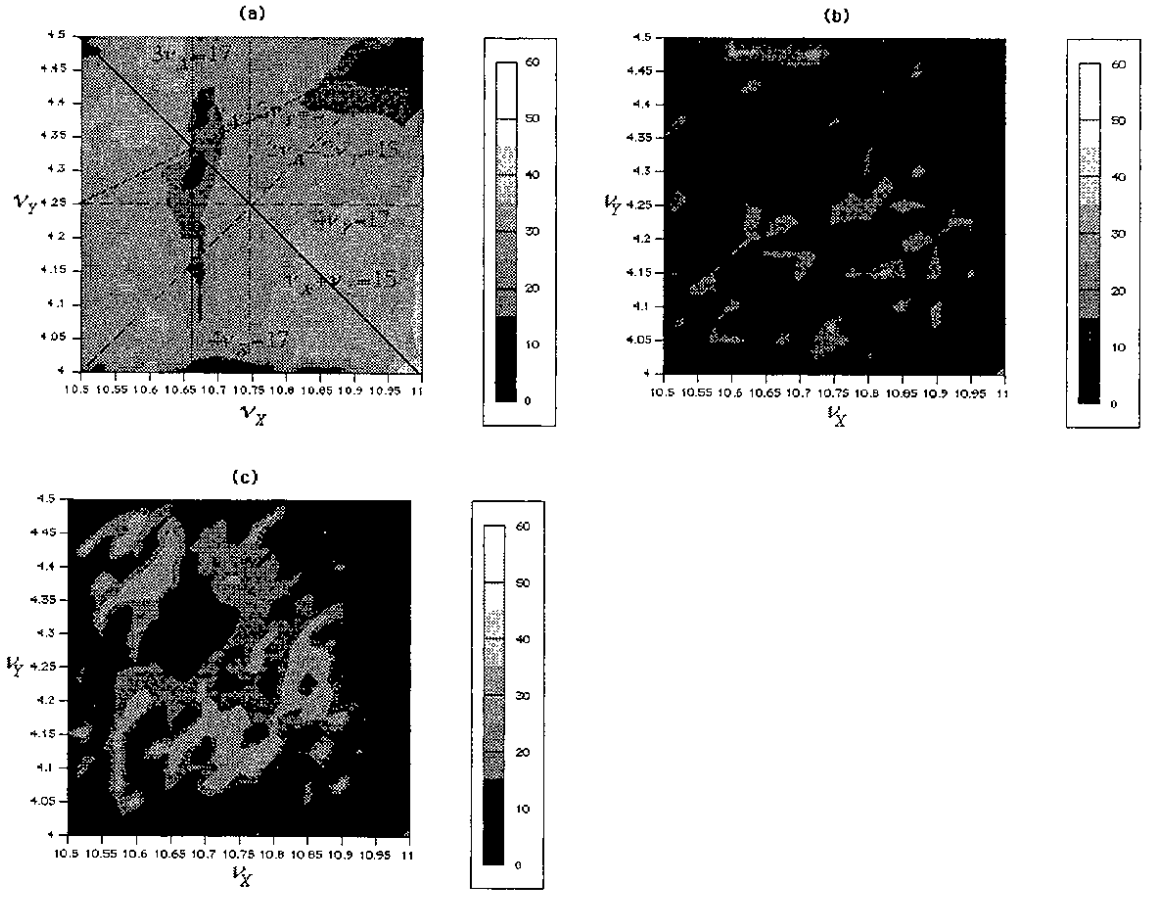

Figure 13: Dynamic apertures for a tune survey in 135° low-emittance cell optics. (a) Without machine errors, (b) with machine errors and (c) after corrections of the COD in (b)

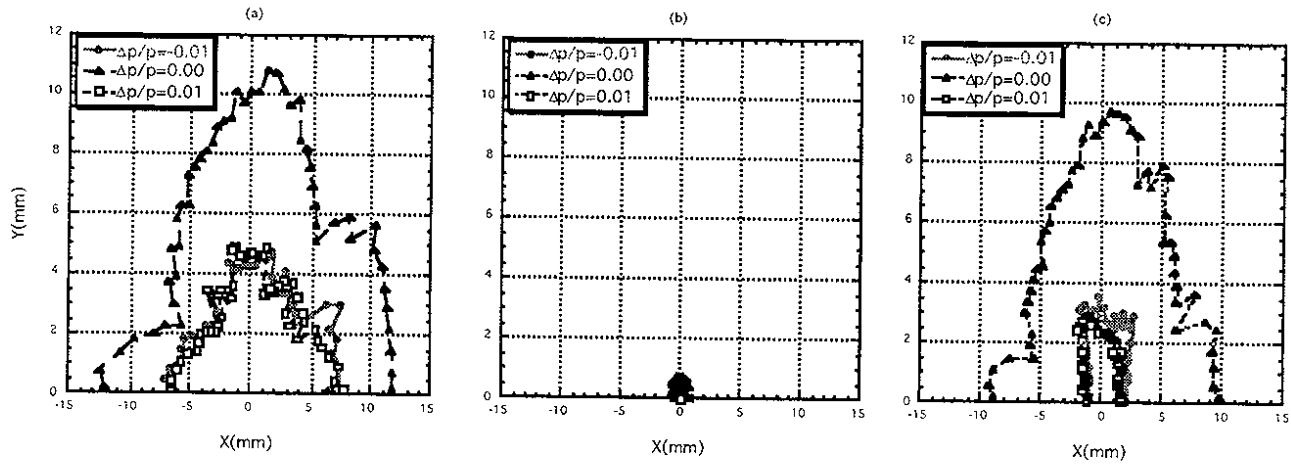

Figure 14: Dynamic apertures at the center of the long straight section in 135° low-emittance cell optics. (a) Without machine errors, (b) with machine errors and (c) after corrections of the COD in machine errors ν_x=10.60 and ν_y=4.35.

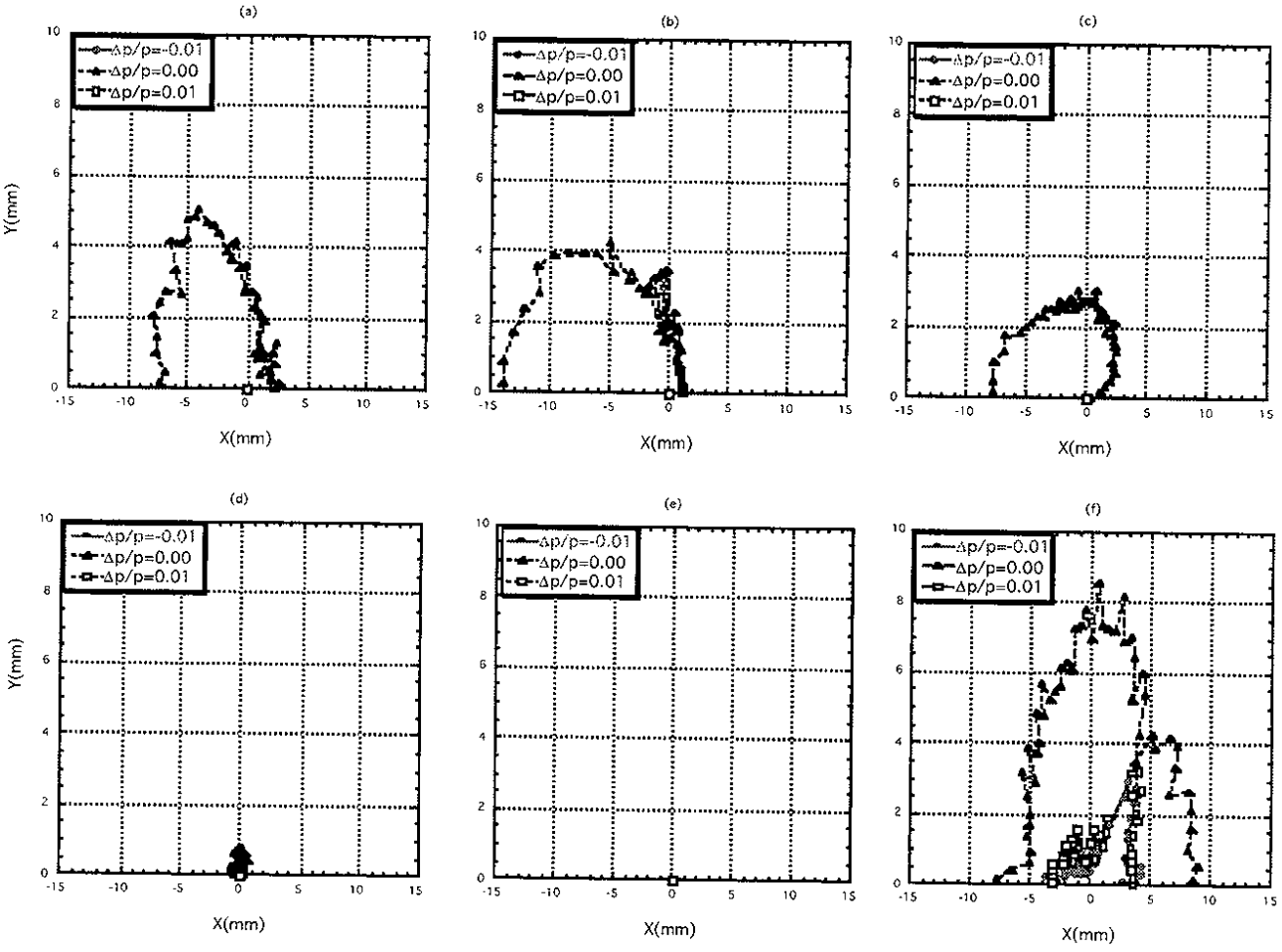

Figure 15: Dynamic apertures at the center of the long straight section in a low-emittance 135° cell. ν_x=10.60 and ν_y=4.35. They show the dependence of the dynamic aperture on the machine errors. (a) Shows the dynamic apertures when the steering error is excluded in machine errors, (b) the rotation error, (c) the magnetic error, (d) the length error, (e) the BPM error and (f) alignment error.

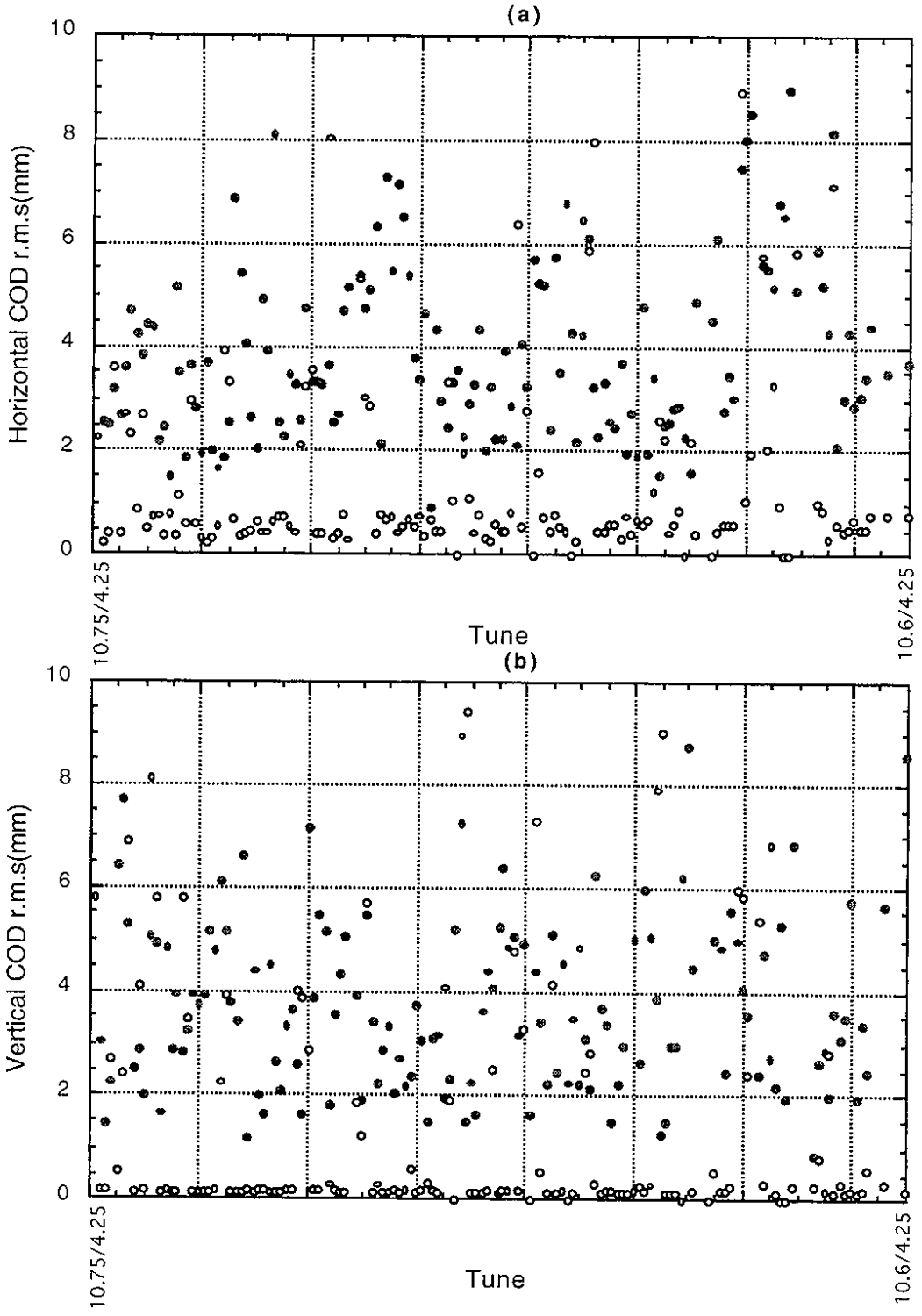

Figure 16: (a) and (b) show the horizontal and vertical COD for the cases of 150 tunes in 135° optics, respectively. Here, the points are the COD when the machine errors are included to an ideal lattice. The circles are the COD after corrections of the COD in points are performed.

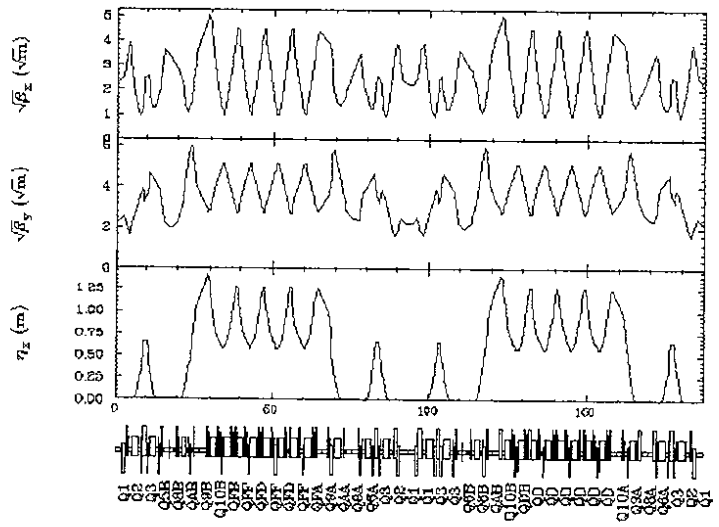

Figure 17: Median-emittance cell and its optical functions.

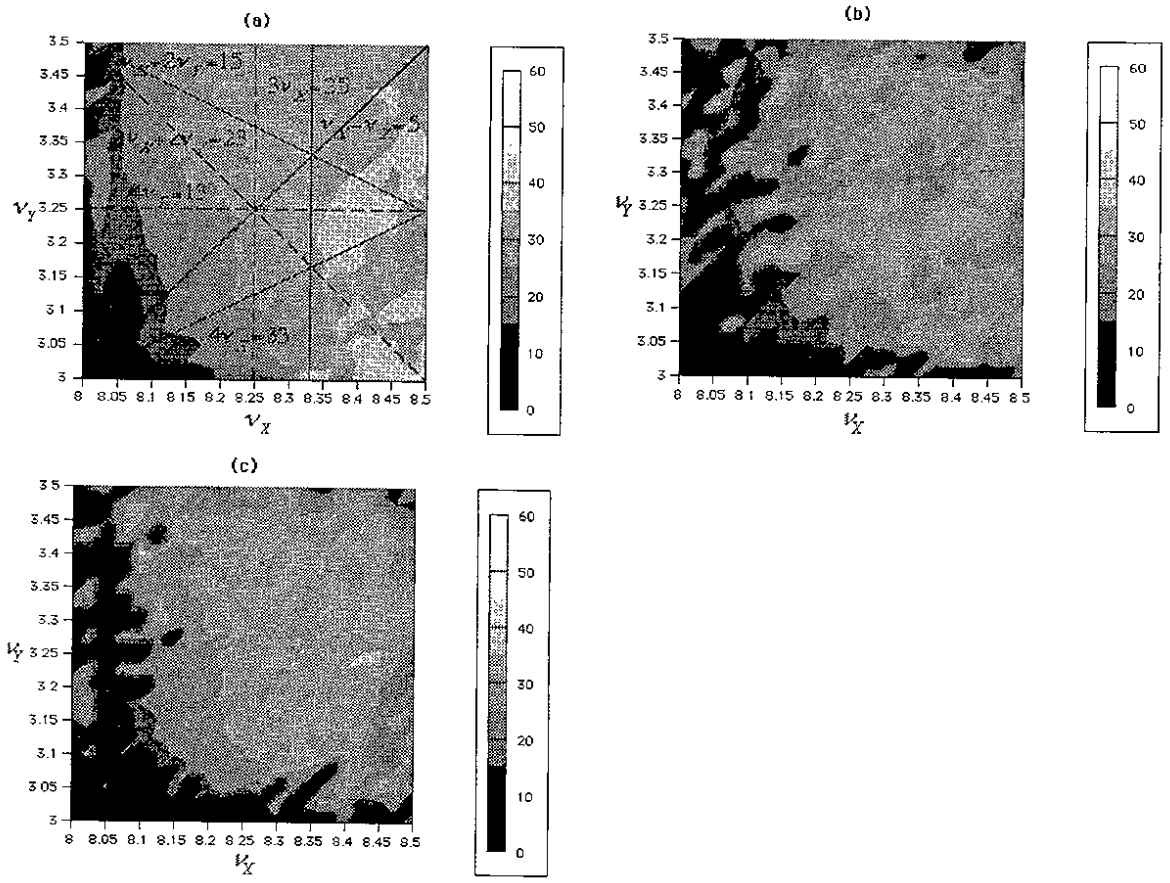

Figure 18: Dynamic apertures for a tune survey in medium-emittance cell optics. (a) Without machine errors, (b) with machine errors and (c) after corrections of COD in (b)

The COD in Figure 14.(c) is adjusted to an r.m.s. error of $0.40mm$ and $0.08mm$ in the horizontal and vertical directions, respectively.

Figures 16.(a) and (b) show the closed orbit distortions in the horizontal and vertical directions for the cases of 150 tunes in 135^o optics, respectively. the points are closed orbit distortions when the machine errors are included to the ideal lattice. The circles are the closed orbit distortions after COD corrections in points are performed. We can see that the COD in Figure 16 is adjusted to r.m.s. errors of 0.5mm and 0.2mm in the horizontal and vertical directions, respectively.

4.4 Medium-Emittance Cell Optics

Figure 17 shows the optics of a medium emittance cell and its optical functions. Figure 18.(a) shows the dynamic apertures for a tune survey in the case that machine errors are not included into the lattice. Figure 18.(b) shows the dynamic apertures with machine errors. Figure 18.(c) shows the dynamic apertures after corrections of the COD are applied in Figure 18.(b). In this optics we can see that the dynamic aperture is totally large compared with those of the low-emittance optics.

Figure 19 shows the dynamic apertures at the center of the long straight section at a tune ν_x=8.45 ν_y=3.325, around which this lattice has a large dynamic aperture.

The closed orbit distortions in Figure 19.(c) are adjusted to r.m.s. errors of 0.31mm and 0.08mm in the horizontal and vertical directions, respectively. We can see that this optics provides a comparative large dynamic apertures compared to low-emittance lattices.

Figures 20.(a) and (b) show the closed orbit distortions in the horizontal and vertical directions for the cases of 150 tunes in medium optics, respectively. The points are closed orbit distortions when the machine errors are included to the ideal lattice. The circles are the closed orbit distortions after corrections of COD in points are performed. The COD in Figure 20 is adjusted to r.m.s. errors of 0.5mm and 0.2mm in the horizontal and vertical directions, respectively.

5 Discussion and Conclusion

Synchrotron light sources for low emittance to produce a high brightness result in very strong sextupole magnets to compensate for chromaticity. This introduce strong nonlinear magnetic fields in the lattices and affects the stable region in transverse phase space. Then, one of the most important issues in this case is that the dynamic aperture becomes smaller due to the fact that the sextupole fields become stronger for the lower emittance optics. If the dynamic aperture is smaller than the physical aperture, it is actually difficult to inject a beam into a ring, which results in a bad beam lifetime. It is necessary to estimate the dynamic aperture of the machine for the successful operation of a ring. Thus, it requires estimate of the effects on the dynamic aperture due to strong sextupoles. Accordingly, we investigated in detail the dynamic aperture for several low-emittance optics in the PF ring. The results of this simulation give an estimation for the requirement that the lattice provides a sufficient dynamic aperture in the PF ring. At the stage of operation, this can provide a information concerning whether the dynamic aperture in each lattice can be smaller than the physical aperture or not. Then, the dynamic aperture in tune space is obtained by particle tracking using the computer code SAD.

Even if the dynamic aperture without machine errors is larger than the physical aperture, beam injection in the starting state of operation may become difficult in the case that the dynamic aperture becomes much smaller due to machine errors. On the other hand, the dynamic aperture can be made larger by performing a correction of the COD. However, a measurement of the COD can only be performed at the stage of beam storage. Accordingly, in a starting state of ring operation, we can correct the steering magnets by using orbit data from a single pass beam position monitor[7]. By performing this work on the entire ring successively, we can correct the COD in a ring and circulate a beam in the ring.

When we estimate the dynamic aperture by the tracking method, the dynamic apertures in 90^o and medium optics with a correction of the COD are considered to be sufficiently large for storage. That of 105^o is almost as small as the dynamic aperture required for storage. On the other hand, the case of 135^o optics totally gives a narrow dynamic aperture and it will be difficult for storage. As a result, we find that 90^o cell optics after a correction of the COD provides a sufficient dynamic aperture in a low-emittance PF ring. In this way, the emittance which can be achieved in a new lattice will have a dependence on the dynamic aperture. This means that detailed operation points must be chosen based on the view point

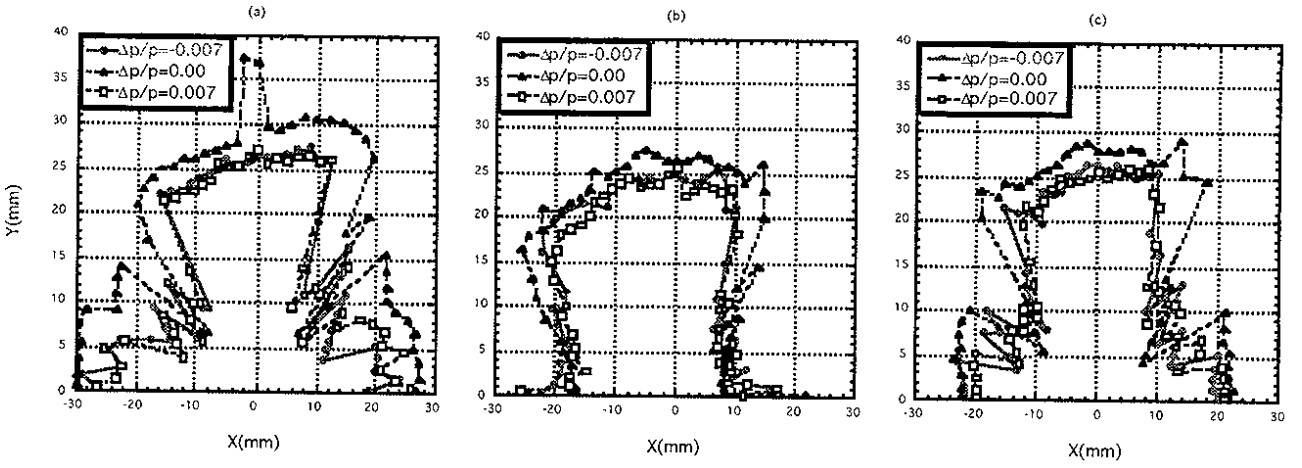

Figure 19: Dynamic apertures at the center of the long straight section in a tune of ν_x=8.45 ν_y=3.325. (a) Without machine errors, (b) with machine errors and (c) after corrections of the COD in (b)

of the dynamic aperture.

It is shown that the horizontal emittance is 100 times larger than the vertical one, and less dependent on machine errors. It is also shown that the vertical emittance is generated by machine errors; in particular, the dymanic aperture is strongly affected by the alignment error among machine errors. In the simulation, we assumed that the machine errors have a Gaussain distribution truncated by 3σ. It is shown that machine errors truncated by 1 σ in its distribution give almost the same result as machine errors truncated to 3σ when we obtain the dynamic aperture. It is shown that COD corrections can be performed better in the vertical direction than the horizontal direction in the PF ring.

Acknowledgements We would like to thank Prof. K.Hirata and Prof.S.Kamada for guidances and useful discussions.

References

[1] M. Katoh et al., Proc. of the 4th European Particle Accelerator Conference (EPAC94), London, 1994, p.636

[2] M. Katoh and Y. Hori, Proc. of the 5th European Particle Accelerator Conference (EPAC96), Barcelona, 1996. p.650

[3] D.Robin et al., AIP Conf. Proc. 344, AIP, New York, 1994

[4] M. Katoh and Y. Hori(ed.), in Japanese, KEK Report 92-20

[5] K.Hirata, An introduction to SAD, Second Advanced ICFA Beam Dynamics Workshop, CERN 88-04 (1988).

[6] A. Ropert, CERN 90-04, 1990

[7] T.Honada et al., Proc. of the 5th European Particle Accelerator Conference (EPAC96), Barcelona, 1966, p.1660

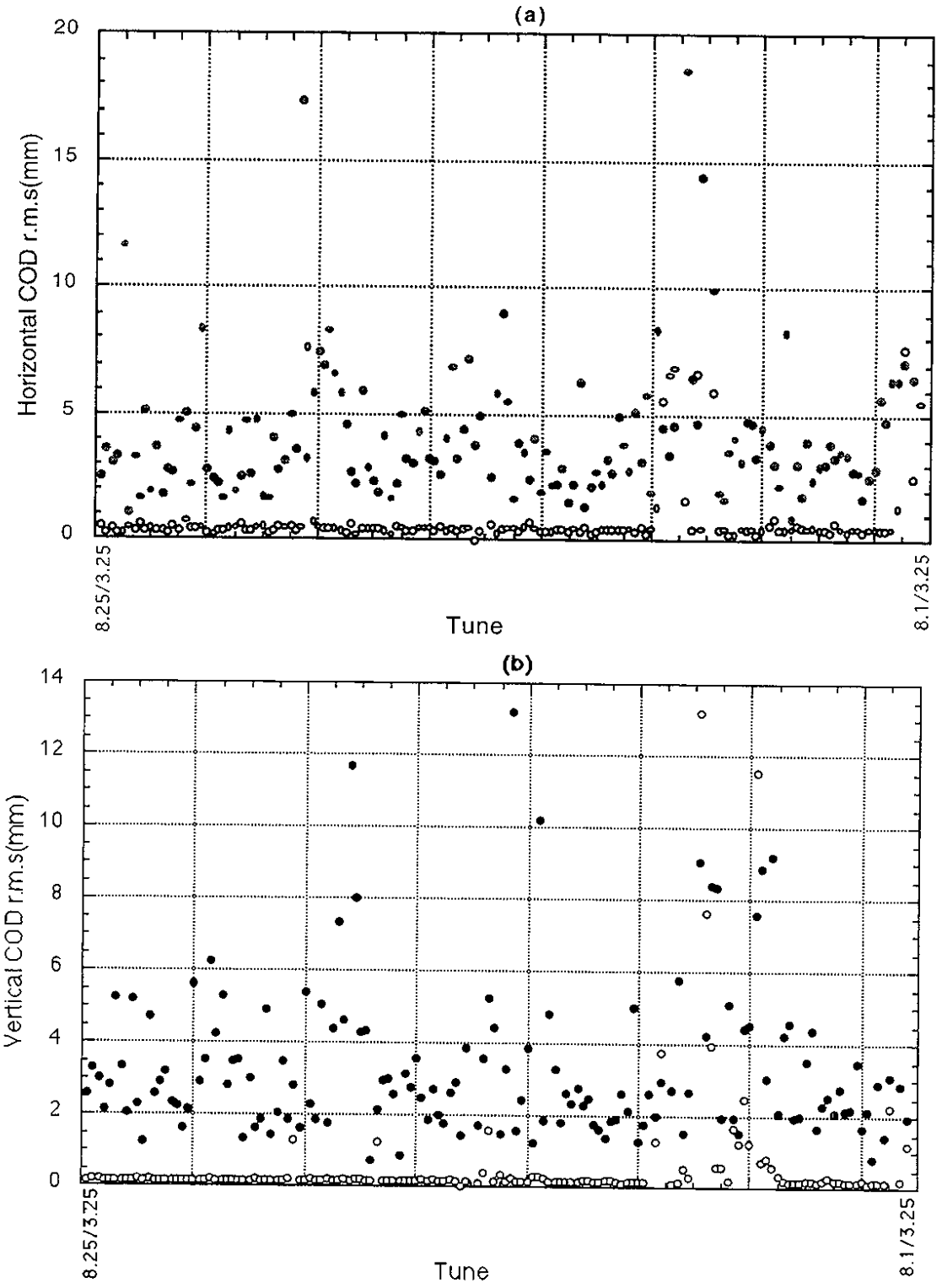

Figure 20: (a) and (b) show the horizontal and vertical COD for the cases of 150 tunes in medium optics, respectively. The points are the COD when the machine errors are included to the ideal lattice. The circles are the COD after corrections of the COD in points are performed.